Batteries & Supercaps

Research Article
doi.org/10.1002/batt.202300074

Chemistry Europe
European Chemical Societies Publishing

www.batteries-supercaps.org

VIP *Very Important Paper*

Refining the Grain Size of Zinc Electrodeposit by Pb^{2+} Ion Grinding for Compact and Stable Zinc Anode

Yang-Feng Cui,[a, c] Ren-Fei Cao,[a, c] Qi Hao,[c] Zhen-Bang Zhuang,[c] Zi-Long Xie,[c] Hao Chen,[c] Kai Li,[c] Qingshuang Wang,[d] Wan-Qiang Liu,*[a] Yingkui Yang,[b] Gang Huang,*[c] and Yunhai Zhu*[b]

Recently, aqueous zinc-based batteries (AZBs) have become a promising candidate for energy storage devices due to the high safety of aqueous electrolytes and the appealing features of Zn anodes, for example, low cost and high theoretical capacity. However, the excessive growth of Zn electrodeposits as well as the uneven stacking of large hexagonal Zn crystal units always render loose and irregular electrodeposition or even dendritic growth, which seriously deteriorates the actual performance of AZBs. Herein, to refine the grain size of Zn electrodeposits, a trace of Pb^{2+} ions as a novel electrolyte additive is performed to inhibit the growth of Zn grain during the Zn electrodeposition. Owing to the higher adsorption energy of Pb^{2+} ions on Zn crystal when compared with Zn^{2+} ions, the strongly positively-charged Pb^{2+} ions are tightly absorbed on the typical crystal planes of initially-formed Zn nuclei, which block the way for the subsequent absorption and electroreduction of Zn^{2+} ions. As a result, the Pb^{2+} ions-containing electrolyte refines the grain size of Zn electrodeposits from 7.43–7.87 μm to 0.88–2.26 μm, and affords a high reversibility of Zn plating/stripping behavior with a high Coulombic efficiency of 99.9% over 1000 cycles.

Introduction

Aqueous zinc-based batteries (AZBs) have drawn a growing attention over the recent years, because of their intrinsic merits, such as the high ionic conductivity, low cost, high security, and environmental benignity of aqueous electrolytes, as well as the cheapness and high theoretical capacity of Zn anode (820 $mAh\,g^{-1}$ or 5855 $mAh\,cm^{-3}$).[1] These appealing features render the AZBs extremely favorable for large-scale energy-storage systems (EESs) that require batteries with low cost and inherent safety.[2] To this end, various AZBs prototypes, for example, Zn-air batteries, Zn-based flow batteries, and Zn-ion batteries, are emerging rapidly, which have made great progresses on both material designs and cell performances but suffer from common challenges originated from notorious Zn anodes (e.g., dendrite growth, Zn corrosion reaction and hydrogen evolution reaction).[3]

To eliminate these Zn anode-involved parasitic reactions and then prolong the lifespan of AZBs, research efforts have been devoted to kinetically optimizing the electrochemical environment for Zn plating/stripping behavior from the perspectives of electrolyte composition regulations, current collectors or anode structures designs, and artificial interface constructions.[1b,4] Among these technical explorations to facilitate durable Zn anode, electrolyte additives have been demonstrated as a facile and effective approach due to its high compatibility to existing batteries fabrication technologies.[5] To date, various electrolyte additives like metallic ions, organic molecules, and polymers have been engaged to regulate Zn plating/stripping behavior, which either serves as electrostatic shielding (e.g., Na^+, Li^+, and diethyl ether) to avoid the growth of Zn dendrites or change electrode/electrolyte interface or solvation structure of Zn^{2+} ion (e.g., polyethyleneimine, triethylphosphate, and glucose) to enhance reaction kinetics for Zn electrodeposition.[5b,6] Despite significant improvements on both lifespan and Zn utilization have been achieved, the excessive growth of Zn crystalline grain along (002) plane are uncontrollable, thus easily forming irregular and loose Zn electrodeposits once the large plate-like Zn grains are built up unevenly. Therefore, controlling the grain size of Zn electrodeposits represents an efficient way to achieve compact and stable Zn anode but remains unfeasible to date, since the overgrowth of hexagonal Zn plane is thermodynamically favorable.[7]

Herein, to refine the grain size of Zn electrodeposits, a trace of Pb^{2+} ions as a novel electrolyte additive were performed to inhibit the growth of Zn crystal during the Zn electrodeposition. Theoretical results indicated that the Pb^{2+} ions were endowed

[a] *Y.-F. Cui, R.-F. Cao, Prof. W.-Q. Liu*
School of Materials Science and Engineering, Changchun University of Science and Technology, Changchun 130022, China
E-mail: wqliu1979@126.com
[b] *Prof. Y. Yang, Prof. Y. Zhu*
State Key Laboratory of New Textile Materials and Advanced Processing Technologies, Wuhan Textile University, Wuhan 430200, China
E-mail: yhzhu@wtu.edu.cn
[c] *Y.-F. Cui, R.-F. Cao, Q. Hao, Z.-B. Zhuang, Z.-L. Xie, H. Chen, K. Li, Prof. G. Huang*
State Key Laboratory of Rare Earth Resource Utilization, Changchun Institute of Applied Chemistry, Chinese Academy of Sciences, Changchun 130022, China
E-mail: ghuang@ciac.ac.cn
[d] *Q. Wang*
Research Center for Nanotechnology, Changchun University of Science and Technology, Changchun 130022, China.

Supporting information for this article is available on the WWW under https://doi.org/10.1002/batt.202300074

Research Article
doi.org/10.1002/batt.202300074
Chemistry Europe
European Chemical Societies Publishing

with higher adsorption energy on Zn crystal when compared with Zn^{2+} ions. As a result, the strongly positively-charged Pb^{2+} ions were tightly absorbed on the typical crystal planes of initially-formed Zn nuclei to prevent the subsequent adsorption and electroreduction of Zn^{2+} ions, thereby refining the grain size of Zn electrodeposits from 7.43–7.87 μm to 0.88–2.26 μm. Importantly, benefiting from the "grinding effect" of Pb^{2+} ions, the Pb^{2+} ions-containing electrolyte afforded a high reversibility of Zn plating/stripping with the high Coulombic efficiency (CE) of 99.9% over 1000 cycles and enabled the mildly aqueous Zn//V_2O_5 cell with durable cycling life over 2000 cycles. This work opens up an efficient strategy to engineering highly reversible Zn anodes by refining the grain size of electrodeposits with a strongly adsorbable ion additive, paving the way for the development of high-performance AZBs.

Results and Discussion

Electrochemical performance of Zn plating/stripping behavior

The Pb^{2+} ions-containing $ZnSO_4$ (ZS + Pb) electrolyte was prepared by dissolving a trace of $PbSO_4$ (~1.4 mM) in a commonly used 2 M $ZnSO_4$ (ZS) electrolyte for AZBs. To verify the function of Pb^{2+} ion additive for Zn anode, we firstly compared the Zn plating/stripping performance in symmetric Zn//Zn cells with ZS and ZS + Pb electrolytes at a low current density of 1 mA cm^{-2} (Figure 1a). Despite the cell with ZS electrolyte showed a gradually decreased voltage hysteresis during the first 74 h, its voltage suffered from the obvious fluctuation after ~223 h and suddenly dropped to nearly 0 V after ~458 h, standing for the potentially soft short and subsequent short circuit, respectively.[8] By contrast, the cell with ZS + Pb electrolyte exhibited a durable lifespan of 600 h with stable voltage hysteresis less than 100 mV. Furthermore, as the current density increased to 20 mA cm^{-2}, the Zn//Zn cell with ZS + Pb electrolyte still demonstrated durable stability of 200 h, corresponding to 2000 cycles, which was much higher than that of the cell in ZS electrolyte (Figure 1b). The cell failure with ZS electrolyte at a high current density may be attributed to the cumulative H_2 caused by the water-induced corrosion, as shown in Figure S1(a) (Supporting Information). And the corrosive by-product of layered double hydroxide (LDH) was also detected after 800 cycles (Figure S1b and c, Supporting Information). It resulted in the poor contact of interior battery, reflecting in the sharp voltage polarization after ~81 h (810 cycles in Figure 1b). Furthermore, to figure out the enhanced reversibility of cell after introducing Pb^{2+} ion additive, the Zn//Zn cells with ZS and ZS + Pb electrolytes after 50 cycles were disassembled to analyze the morphology of Zn electrodes by a scanning electron microscopy (SEM, Figure S2, Supporting Information). It was observed that Zn electrodes in ZS electrolyte showed irregular electrodeposits and

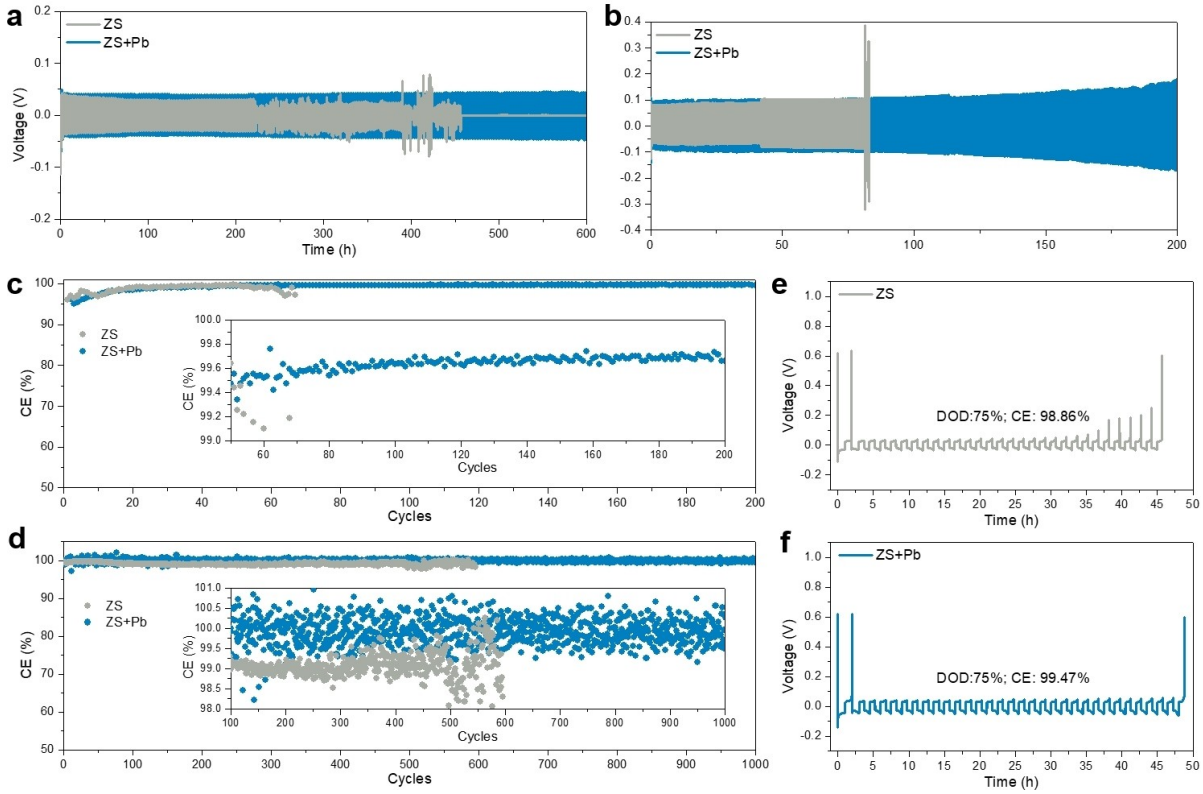

Figure 1. a, b) Cycling performance of the Zn//Zn cells in different electrolytes with a fixed areal capacity of 1 mAh cm^{-2} at a) low current density of 1 mA cm^{-2} and b) high current density of 20 mA cm^{-2}. c, d) CE plots of Zn plating/stripping behavior using the Zn//Cu cells in different electrolytes at current densities of c) 1 mA cm^{-2} and d) 20 mA cm^{-2} with an areal capacity of 1 mAh cm^{-2} and stripping cut-off voltage of 0.6 V. e, f) Voltage profiles of Zn plating/stripping with DOD of 50% in e) ZS and f) ZS + Pb electrolytes on a Cu electrode at a current density of 4 mA cm^{-2}.

Research Article
doi.org/10.1002/batt.202300074
Chemistry Europe
European Chemical Societies Publishing

dendritic formation, whereas the Zn electrodes in ZS + Pb electrolyte demonstrated smooth morphology, thereby affording a prolonged cycle life.

Given that the reversibility of Zn anode was of great significance for practical implementation of rechargeable AZBs, the CE tests were performed to evaluate the Zn plating/stripping efficiency (Figure 1c–f). As shown in Figure 1(c), the control cell with ZS electrolyte afforded the poor reversibility at a current density of 1 mA cm^{-2}, which showed an unsatisfied lifespan of 70 cycles with fluctuation of the CE at the end of cycle life. When the ZS + Pb electrolyte was used, the cell displayed stable plating/stripping behavior over 200 cycles with an average CE of 99.6% (Figure 1c). Such improvement effects were also verified at the high current density (20 mA cm^{-2}), the Zn//Cu cell with ZS + Pb electrolyte demonstrated superior reversibility (average CE of 99.9% over 1000 cycles) than the control cell with ZS electrolyte (average CE of 99.2%), as shown in Figure 1(d). A "reservoir half-cell" method introduced by Aurbach et al. was further adopted to evaluate the CE.[9] The results indicated that Zn plating/stripping behavior in ZS + Pb electrolyte still exhibited the higher CE of > 99% at different discharge of depth (DOD) than those ones in ZS electrolyte (Figure 1e and f, and Figure S3, Supporting Information). This enhanced stability and reversibility reveal the fact that Pb^{2+} ions are likely to regulate Zn plating/stripping behavior, thereby enabling durable Zn anode.

Morphological and structural analysis

To investigate how the Pb^{2+} ions affected the Zn electrodeposition behavior, we studied the morphology revolution for Zn electrodeposits in ZS and ZS + Pb electrolytes at various current densities with a fixed areal capacity of 3 mAh cm^{-2} on Ti foil (Figure S4, Supporting Information). As the ex situ SEM images shown in Figure 2a–d, all the Zn electrodeposits were

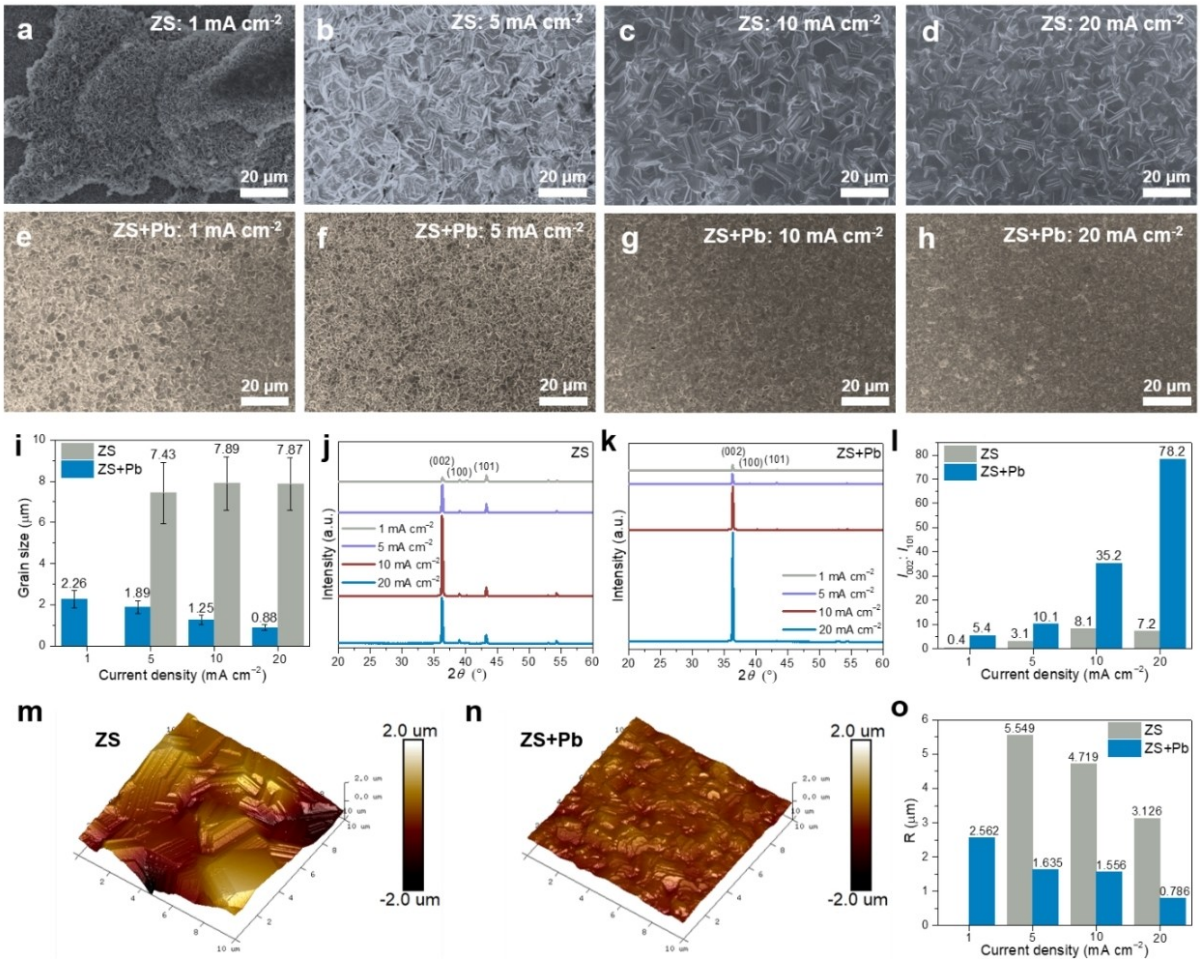

Figure 2. a–h) SEM images of Zn electrodeposits on Ti foil using a–d) ZS and e–h) ZS + Pb electrolytes with an areal capacity of 3 mAh cm^{-2} and different current densities of a and e) 1 mA cm^{-2}, b and f) 5 mA cm^{-2}, c and g) 10 mA cm^{-2}, and d and h) 20 mA cm^{-2}. i) The grain sizes of Zn electrodeposit with ZS and ZS + Pb electrolytes under different current densities (the grain sizes are mean values, and error bars represent the standard deviation of ~50 determinations, obtained from the Figures S6 and S7, Supporting Information). j and k) XRD patterns obtained from the Zn electrodeposition on Ti foil under the different current densities and a fixed areal capacity of 3 mAh cm^{-2} with j) ZS and k) ZS + Pb electrolytes, and l) the corresponding I_{002}:I_{101}. m and n) AFM height images of Zn deposits at a fixed areal capacity of 3 mAh cm^{-2} and current density of 20 mA cm^{-2} in m) ZS and n) ZS + Pb electrolytes. e) *R* of Zn electrodeposits in ZS and ZS + Pb electrolytes with increasing current density (the surface of Zn electrodeposit in ZS electrolyte at a low current density of 1 mA cm^{-2} was too rough to be used for AFM).

built with the hexagonal Zn crystal grains in ZS electrolyte, but were diverse as the increased current densities, including irregularly plate-like deposits at a low current density (1 mA cm^{-2} in Figure 2a, and Figure S5a, Supporting Information), plate-stacked blocks at a moderate current density (5 mA cm^{-2} in Figure 2b, and Figure S5b, Supporting Information), and the compactly plate-stacked texture at the high current densities (10 and 20 mA cm^{-2} in Figure 2c and d, and Figure S5c and d, Supporting Information). These conclusions are corresponded to the most reported results that the Zn electrodeposits tend to form large hexagonal plates along (002) plane as this trend is thermodynamically favorable.[7,10] Although the dense Zn electrodeposits are able to be formed at the high current densities, the current-dependent regulation strategy is powerless to fundamentally solve the challenges facing Zn anode.[11] Fortunately, the Zn electrodeposits in such a Pb^{2+} ion-containing electrolyte were consisted of refined Zn grains at whatever current densities, thereby weaving compact and smooth electrodeposits under all test conditions (Figure 2e–h, and Figure S5e–h, Supporting Information).

Considering that the correlation between the microscopic Zn units and the macroscopic stacked Zn electrodeposits, we further analyzed the grain sizes of Zn electrodeposits by measuring the diameter of hexagonal Zn grains in ZS and ZS + Pb electrolytes (Figures S6 and S7, Supporting Information). Given that there were abundant vertical alignment of Zn electrodeposits in ZS electrolyte at the current density of 1 mA cm^{-2}, the grain size under this condition was inaccessible from SEM images and then was not taken into consideration. As shown in Figure 2(i), the grain size of Zn deposits in ZS system ranged from 7.43 to 7.89 μm, while the Zn grains formed in ZS + Pb system were much smaller, which possessed a size of 2.26, 1.89, 1.25, and 0.88 μm at the current densities of 1, 5, 10, and 20 mA cm^{-2}, respectively.

X-ray diffraction (XRD) was carried out to find out the deposition orientations. In ZS electrolyte, the Zn electrodeposits showed the relatively strong (101) orientation at the low current density but the relatively strong (002) orientation at the high current density (Figure 2j), which actually experienced a series of current-induced morphology evolution from irregular plate-like deposit to plate-stacked texture with enhanced current density (see details in our previous work[11]). In this process, the enhanced (002) peak intensity meant that there were more plate-like (002) planes parallel to the substrate. In comparison, the grain-refined electrodeposits in ZS + Pb electrolyte consistently exhibited horizontal alignment, reflecting in the strong (002) peaks of XRD patterns at any current densities (Figure 2k). For a more intuitive analysis, the difference between deposition orientations in ZS and ZS + Pb systems could be quantified by the peak intensity ratio between (002) and (101) (denoted as I_{002}:I_{101}),[12] in which the I_{002}:I_{101} represented the ratio between horizontal and vertical alignment of plate-like electrodeposits. As shown in Figure 2(l), the I_{002}:I_{101} in ZS system showed a maximum value of 8.1 at the current density of 10 mA cm^{-2}, whereas, under the effect of Pb^{2+} ions, the I_{002}:I_{101} increased sharply from 5.4 to 78.2 as current density increased from 1 mA cm^{-2} to 20 mA cm^{-2}. It indicated that the Zn electrodeposits with smaller grain sizes prefer to be parallel to the substrate when compared with the large plate-like electrodeposits, thus contributing to the smooth electrodeposition morphology.

To strengthen this conclusion, the three-dimensional morphology analysis from atomic force microscope (AFM) was performed for all Zn electrodeposits. In ZS system, the AFM images showed the rough surfaces of Zn electrodeposits that consisted of the large grains (Figure 2m, and Figure S8, Supporting Information). In contrast, the grain-refined electrodeposits induced by Pb^{2+} ion additive showed smooth surfaces (Figure 2n, and Figure S9, Supporting Information). The roughness (R) from AFM images recorded in the above two electrolytes was plotted versus current density (Figure 2o), in which R was highly correlated with grain size. Even though the Zn electrodeposition in ZS electrolyte adopted the compactly plate-stacked texture at the high current densities (10 mA cm^{-2} and 20 mA cm^{-2}), it was also troubled by the high R of 4.719 and 3.126 μm, since it was made up of large plate-like grains. By contrast, the Zn deposits with grain-refined particles demonstrated smaller R, which showed the pretty low R of 2.562 μm, 1.635 μm, 1.556 μm, and 0.786 μm at 1, 5, 10 and 20 mA cm^{-2}, respectively. Therefore, the refined Zn grains with smaller sizes preferred to build smoother Zn electrodeposits.

Zn electrodeposition mechanism with/without Pb^{2+}

To figure out how the Pb^{2+} ions affected the Zn electrodeposition behavior, we first studied the Zn electrodeposits in ZS and ZS + Pb electrolytes with energy-dispersive X-ray spectroscopy (EDS). As shown in Figure 3(a) and Figure S10 (Supporting Information), the Zn and O element but no Pb element were detected in both Zn electrodeposits with ZS and ZS + Pb electrolytes. The absence of the Pb element signal suggested that the Pb^{2+} ions in ZS + Pb electrolyte were not reduced during Zn deposition. And the XRD patterns of Zn electrodeposits further confirmed that there was no Pb metal or Zn-Pb alloy formation (Figure 2k). The quantification of Pb^{2+} concentration in ZS + Pb electrolyte by inductively coupled plasma optical emission spectroscopy (ICP-OES) suggested that Pb^{2+} ions were not involved in Zn electrodeposition, since there was no obvious concentration change of Pb^{2+} ion in ZS + Pb electrolyte before and after electrodeposition (Table S1, Supporting Information). Therefore, we speculated that the Pb deposition behavior is a sluggish kinetic reaction in neutral electrolyte. It is quite distinct from the Pb^{2+} ions-induced Zn electrodeposition mechanism in alkaline and acidic electrolytes, wherein the Pb^{2+} ions and Zn^{2+} ions occurred co-deposition reaction (Figure S11, Supporting Information) to optimize Zn deposition behavior.[13]

Chronoamperometry (CA) was employed to characterize the Zn nucleation and growth behavior in ZS and ZS + Pb electrolytes. The variation in current density at a constant potential reflected the change in surface morphology during electrodeposition, and a current rise implied an increase in surface area.[14] As shown in Figure 3(b), the current density of Zn deposition in ZS electrolyte increased continuously within

Research Article
doi.org/10.1002/batt.202300074
Chemistry Europe
European Chemical Societies Publishing

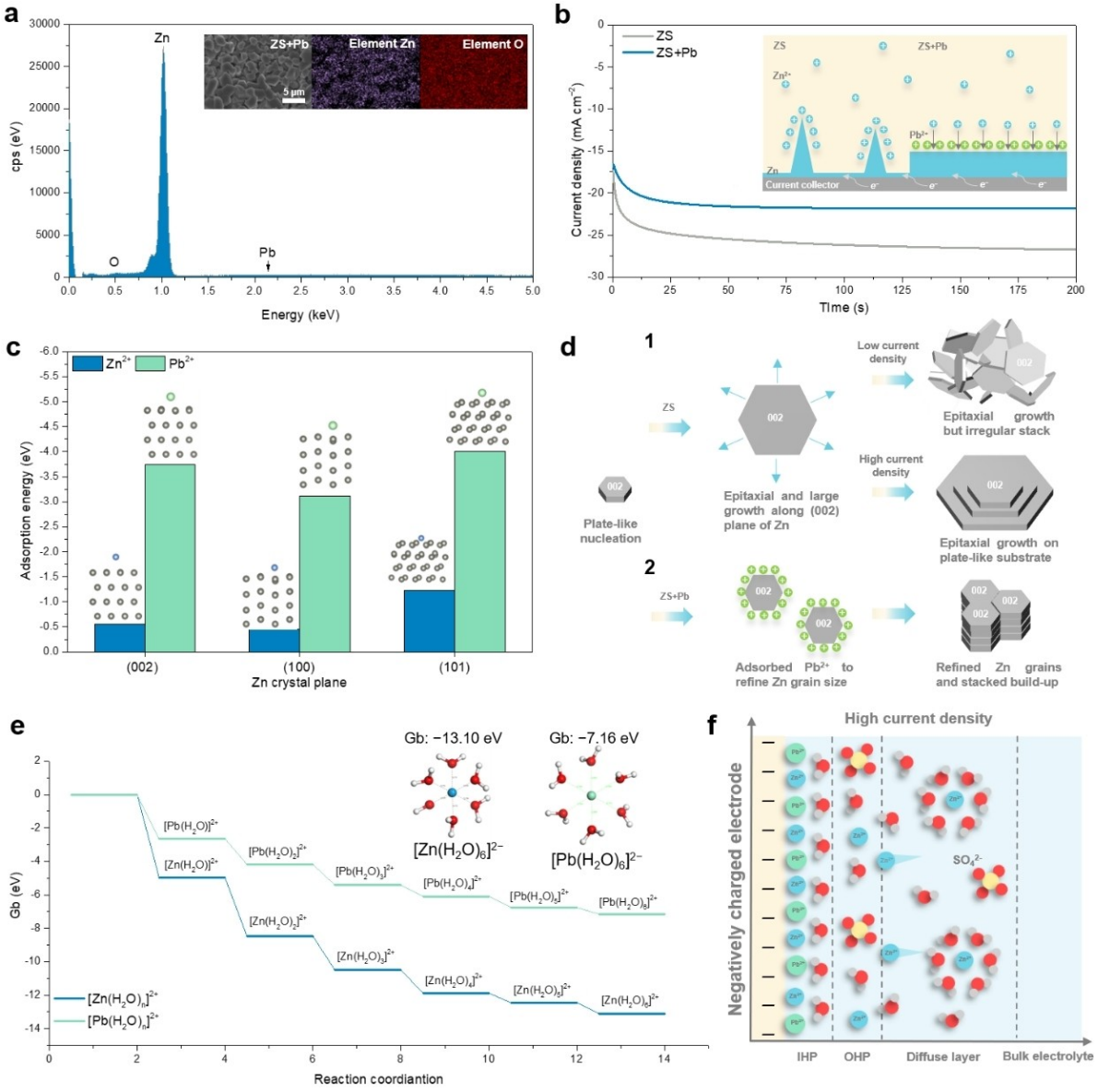

Figure 3. a) EDS pattern of plated Zn on Ti foil using ZS + Pb electrolyte at an areal capacity of 1 mAh cm^{-2} and a current density of 5 mA cm^{-2}. Inset: corresponding EDS mapping images. b) CA during Zn plating process using the Zn//Ti cells with an Ag/AgCl reference electrode in ZS and ZS + Pb electrolytes at an overpotential of −150 mV. Inset: schematic of Zn deposition process. c) Adsorption energies of Zn^{2+} ion and Pb^{2+} ion on (002), (100), and (101) planes of Zn crystal. Insets: optimized structures of Zn^{2+} ion and Pb^{2+} ion adsorption on different crystal planes of Zn. d) Schematic of Zn deposition behavior with and without Pb^{2+} additive. e) ΔG profiles of Zn^{2+} ion and Pb^{2+} ion with H_2O. Insets: optimized geometries and corresponding ΔG for the solvated $[Zn(H_2O)_6]^{2+}$ and $[Pb(H_2O)_6]^{2+}$. f) Schematic of EDL structure at high current density in ZS + Pb electrolyte. The IHP and OHP are the inner Helmholtz layer and outside Helmholtz layer, respectively.

200 s at −150 mV, suggesting a propagation of rough Zn deposition due to the "tip effect" (inset of Figure 3b).[15] In general, Zn^{2+} ions tend to laterally diffuse along the Zn surface to minimize the surface energy and surface area, so that the protuberant and dendritic sites are more energetically favorable for Zn growth (inset in Figure 3b).[16] By contrast, the Zn electrodeposition with ZS + Pb electrolyte exhibited a steady current response after a current increase at the initial nucleation stage within 50s, corresponding to the typical 3D diffusion that the Zn^{2+} ions performed the even movement on the flat Zn surface. It indicated that the Pb^{2+} ions in ZS + Pb electrolytes changed the diffusion behaviors of Zn^{2+} ions from 2D diffusion to 3D diffusion (inset in Figure 3b). Such alteration may be attributed to the strong interfacial adsorption of Pb^{2+} ions, which impeded the 2D diffusion of Zn^{2+} ions across the Zn surface by inflicting an additional energy barrier for lateral movement of Zn^{2+} ions, thereby inhibiting the "tip effect".

To verify the above assumption, the density functional theory (DFT) calculation was employed to calculate the adsorption energies of Zn^{2+} ions and Pb^{2+} ions on representative (002), (100) and (101) planes of Zn crystal. The side view of the adsorbed ions on different crystal planes and the corresponding adsorption energies were shown in Figure 3(c). The adsorption energy between Zn^{2+} ion and (101) plane was

Research Article
doi.org/10.1002/batt.202300074
Chemistry Europe
European Chemical Societies Publishing

−1.2289 eV, which was higher than that of (002) plane (−0.5550 eV) and (101) plane (−0.4544 eV). The preferential adsorption of Zn^{2+} ion on (101) plane supported the epitaxial grain growth along the (002) plane (Figure 3d). By contrast, the adsorption energies for Pb^{2+} ion on (002), (100) and (101) planes were calculated to be −3.7482 eV, −3.1122 eV and −4.0136 eV, respectively, which were much higher than that of Zn^{2+} ion (Figure 3c). Precisely because of the strong adsorption ability of Pb^{2+} ion, the strongly positively-charged Pb^{2+} ions were tightly absorbed on the typical crystal surfaces of initially-formed Zn nucleus (Figure 3d). Besides, the calculated Gibbs free energy (ΔG) of $[Pb(H_2O)_n]^{2+}$ (n = 1–6, Figure 3e) complexes were lower than those of $[Zn(H_2O)_n]^{2+}$ (n = 1–6, Figure 3e), thus exhibiting the longer bond length (~2.70 Å) of $[Pb(H_2O)_6]^{2+}$ than the bond length (~2.17 Å) of $[Zn(H_2O)_6]^{2+}$. It suggested that the Pb^{2+} ions could more easily get rid of the Pb^{2+}–H_2O interaction, and first enter the inner Helmholtz layer (IHP) of EDL. As a result, the Pb^{2+} ions are enriched in IHP and tightly adsorb on the electrode surface, which will be more prominent as the current increased. (Figure 3f, and Figure S12, Supporting Information).[17] Notably, the strong adsorption of Pb^{2+} ions on both Zn crystals and electrode surfaces may block the way for the subsequent absorption and electroreduction of Zn^{2+} ions, resulting in the grain-refined Zn units with compactly stacked build-up (Figure 3d). Importantly, such strong adsorption could also suppress the electrochemical corrosion of Zn anode in aqueous electrolyte, since the corrosion current in ZS + Pb electrolytes was much smaller than that of in ZS electrolytes (Figure S13, Supporting Information).

The full Zn//V_2O_5 cell performance

A full cell was assembled by pairing Zn anode with V_2O_5 cathode to evaluate the feasibility of the Pb^{2+} ions-containing electrolyte in practical applications. Here, the V_2O_5 cathode material was prepared by ball-milling of commercially available V_2O_5 powder and graphite.[18] The full cells cycled with ZS and ZS + Pb electrolytes at different current densities were shown in Figure 4(a). Compared with the Zn//V_2O_5 cell with ZS electrolyte, the cell with ZS + Pb electrolyte achieved the slightly higher capacities of 430, 392, 353, 279, and 163 mAh g^{-1} at the current densities of 0.5, 1, 2, 3, and 4 A g^{-1}, respectively. This improvement of rate capability from 0.5 to 4 A g^{-1} could be attributed to the enhanced reversibility of grain-refined Zn anode induced by Pb^{2+} ions, and the cell with ZS + Pb electrolyte after cycling with enhanced current density could still recover a high specific capacity of 400 mAh g^{-1} at a low current density of 0.2 A g^{-1} (Figure 4b). Additionally, the cycle stability of Zn//V_2O_5 cells with ZS and ZS + Pb electrolytes were further investigated at a current density of 2 A g^{-1} (Figure 4c). Obviously, the full cell with ZS electrolyte rapidly failed after 420 cycles with a low-capacity retention of 60%, suggesting the poor reversibility of coarse Zn anode with potential parasitic reactions in ZS electrolyte. In contrast, the full cell with ZS + Pb electrolyte retained a highly reversible capacity of 197 mAh g^{-1} after 2000 cycles. This enhancement in long-term cycling performance further confirmed the feasibility of grain-refined Zn anode for practical applications.

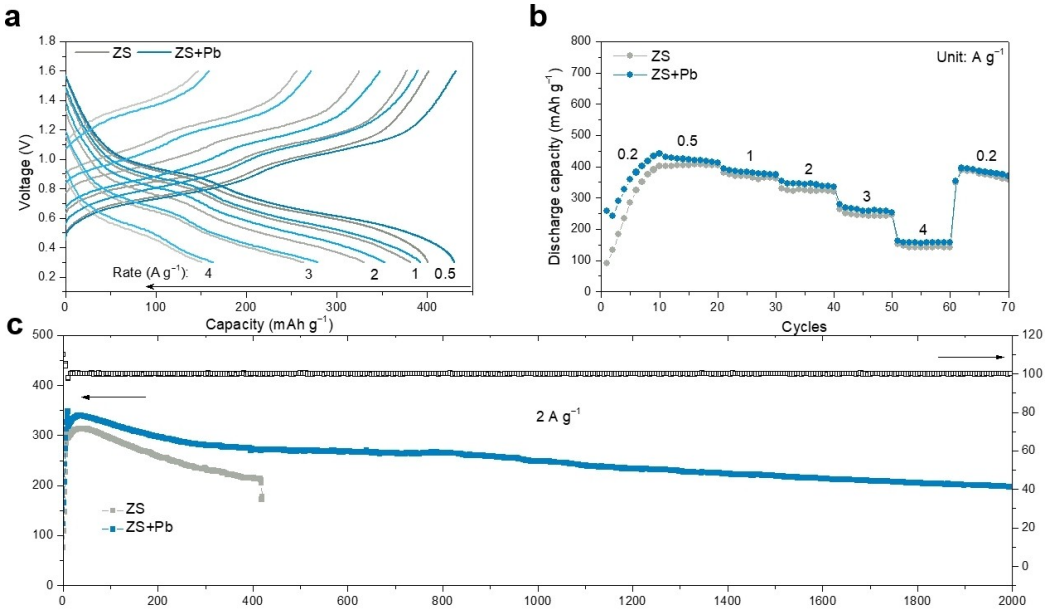

Figure 4. a) Discharge/charge curves and b) rate capability of Zn//V_2O_5 cells with ZS and ZS + Pb electrolytes at different current densities. c) Cycling performance of Zn//V_2O_5 cells with ZS and ZS + Pb electrolytes at a current density of 2 A g^{-1} after the initial activation of 10 cycles at a current density of 0.2 A g^{-1}.

Conclusions

In summary, we have developed a grain refinement strategy to realize the smooth Zn electrodeposition via the introduction of trace Pb^{2+} ions in ZS electrolyte. Owing to the strong adsorption ability of Pb^{2+} ions on the Zn crystal, the strongly positively-charged Pb^{2+} ions were tightly absorbed on the typical crystal planes of initially-formed Zn nuclei, which suppressed the subsequent absorption and electroreduction of Zn^{2+} ions. As a result, the Pb^{2+} ions-containing electrolyte that was endowed with "grinding effect" for electrodeposits refined the Zn grain size from 7.43–7.87 μm to 0.88–2.26 μm, thereby forming smooth Zn electrodeposits. Importantly, the grain-refined Zn anode afforded a high reversibility of Zn plating/stripping behavior with a high CE of 99.9% over 1000 cycles and enabled the mildly aqueous Zn//V_2O_5 cell with durable lifespan over 2000 cycles. This work will provide a novel strategy to realize the compact and stable metal anodes by refining the grain size of electrodeposits via introducing the adsorbable ion with "grinding effect".

Supporting Information

Supporting Information is available from the Wiley Online Library or from the author.

Acknowledgements

This work was financially supported by the National Key R&D Program of China (2017YFE0198100). Supercomputing USTC and Network and Computing Center, Changchun Institute of Applied Chemistry, and Chinese Academy of Sciences are acknowledged for computational support.

Conflict of Interests

The authors declare no conflict of interest.

Data Availability Statement

The data that support the findings of this study are available from the corresponding author upon reasonable request.

Keywords: Pb^{2+} ion additive · grain refinement · Zn anode · aqueous Zn battery

[1] a) G. Zampardi, F. La Mantia, *Nat. Commun.* **2022**, *13*, 687; b) Y. Zou, X. Yang, L. Shen, Y. Su, Z. Chen, X. Gao, J. Zhou, J. Sun, *Energy Environ. Sci.* **2022**, *15*, 5017; c) X. Jia, C. Liu, Z. G. Neale, J. Yang, G. Cao, *Chem. Rev.* **2020**, *120*, 7795.
[2] a) Z. Zhu, T. Jiang, M. Ali, Y. Meng, Y. Jin, Y. Cui, W. Chen, *Chem. Rev.* **2022**, *122*, 16610; b) T. Zhang, Y. Tang, S. Guo, X. Cao, A. Pan, G. Fang, J. Zhou, S. Liang, *Energy Environ. Sci.* **2020**, *13*, 4625; c) Y.-F. Cui, Y.-H. Zhu, J.-Y. Du, Y.-L. Zhang, K. Li, W.-Q. Liu, G. Huang, X.-B. Zhang, *Joule* **2022**, *6*, 1617; d) Y. F. Cui, Z. B. Zhuang, Z. L. Xie, R. F. Cao, Q. Hao, N. Zhang, W. Q. Liu, Y. H. Zhu, G. Huang, *ACS Nano* **2022**, *16*, 20730; e) Y.-H. Zhu, Y.-F. Cui, Z.-L. Xie, Z.-B. Zhuang, G. Huang, X.-B. Zhang, *Nat. Chem. Rev.* **2022**, *6*, 505.
[3] Y. Liu, X. Lu, F. Lai, T. Liu, P. R. Shearing, I. P. Parkin, G. He, D. J. L. Brett, *Joule* **2021**, *5*, 2845.
[4] a) J. Cao, D. Zhang, X. Zhang, Z. Zeng, J. Qin, Y. Huang, *Energy Environ. Sci.* **2022**, *15*, 499; b) L. Zhang, Y. Hou, *Adv. Energy Mater.* **2021**, *11*, 2003823; c) J. Zheng, Q. Zhao, T. Tang, J. Yin, C. D. Quilty, G. D. Renderos, X. Liu, Y. Deng, L. Wang, D. C. Bock, C. Jaye, D. Zhang, E. S. Takeuchi, K. J. Takeuchi, A. C. Marschilok, L. A. Archer, *Science* **2019**, *366*, 645; d) M. Zhou, S. Guo, J. Li, X. Luo, Z. Liu, T. Zhang, X. Cao, M. Long, B. Lu, A. Pan, G. Fang, J. Zhou, S. Liang, *Adv. Mater.* **2021**, *33*, 2100187; e) W. Zhang, Q. Zhao, Y. Hou, Z. Shen, L. Fan, S. Zhou, Y. LU, L. A. Archer, *Sci. Adv.* **2021**, *7*, eabl3752; f) L. Yuan, J. Hao, B. Johannessen, C. Ye, F. Yang, C. Wu, S.-X. Dou, H.-K. Liu, S.-Z. Qiao, *eScience* **2023**, DOI: 10.1016/j.esci.2023.100096.
[5] a) S. Guo, L. Qin, T. Zhang, M. Zhou, J. Zhou, G. Fang, S. Liang, *Energy Storage Mater.* **2021**, *34*, 545; b) Y. Geng, L. Pan, Z. Peng, Z. Sun, H. Lin, C. Mao, L. Wang, L. Dai, H. Liu, K. Pan, X. Wu, Q. Zhang, Z. He, *Energy Storage Mater.* **2022**, *51*, 733; c) C. Zhai, D. Zhao, Y. He, H. Huang, B. Chen, X. Wang, Z. Guo, *Batteries* **2022**, *8*; d) Q. Zhang, J. Luan, X. Huang, L. Zhu, Y. Tang, X. Ji, H. Wang, *Small* **2020**, *16*, 2000929; e) J. Cao, D. Zhang, C. Gu, X. Wang, S. Wang, X. Zhang, J. Qin, Z. S. Wu, *Adv. Energy Mater.* **2021**, *11*, 2101299.
[6] a) F. Wan, L. Zhang, X. Dai, X. Wang, Z. Niu, J. Chen, *Nat. Commun.* **2018**, *9*, 1656; b) X. Guo, Z. Zhang, J. Li, N. Luo, G.-L. Chai, T. S. Miller, F. Lai, P. Shearing, D. J. L. Brett, D. Han, Z. Weng, G. He, I. P. Parkin, *ACS Energy Lett.* **2021**, *6*, 395; c) W. Xu, K. Zhao, W. Huo, Y. Wang, G. Yao, X. Gu, H. Cheng, L. Mai, C. Hu, X. Wang, *Nano Energy* **2019**, *62*, 275; d) S. Liu, J. Mao, W. K. Pang, J. Vongsvivut, X. Zeng, L. Thomsen, Y. Wang, J. Liu, D. Li, Z. Guo, *Adv. Funct. Mater.* **2021**, *31*, 2104281; e) A. Bani Hashemi, G. Kasiri, F. La Mantia, *Electrochim. Acta* **2017**, *258*, 703.
[7] J. Zheng, L. A. Archer, *Sci. Adv.* **2021**, *7*, eabe0219.
[8] Q. Li, A. Chen, D. Wang, Z. Pei, C. Zhi, *Joule* **2022**, *6*, 273.
[9] a) D. Aurbach, Y. Gofer, *J. Electrochem. Soc.* **1991**, *138*, 3529; b) B. D. Adams, J. Zheng, X. Ren, W. Xu, J.-G. Zhang, *Adv. Energy Mater.* **2018**, *8*, 1702097; c) L. Ma, M. A. Schroeder, O. Borodin, T. P. Pollard, M. S. Ding, C. Wang, K. Xu, *Nat. Energy* **2020**, *5*, 743.
[10] L. K. Moghaddam, S. R. Paschepari, M. A. Zaimy, A. Abdalaian, A. Jebali, *Sci. Data* **2016**, *3*, 160080.
[11] Y.-F. Cui, R.-F. Cao, J. Du, Z.-B. Zhuang, Z.-L. Xie, Q.-S. Wang, D. Bao, W. Liu, Y. Zhu, G. Huang, *Chem. Commun.* **2023**, *59*, 2437.
[12] J. C. Zheng, J. F. Yin, D. H. Zhang, G. J. Li, D. C. Bock, T. Tang, Q. Zhao, X. T. Liu, A. Warren, Y. Deng, S. Jin, A. Marschilok, E. S. Takeuchi, K. J. Takeuchi, C. D. Rahn, L. A. Archer, *Sci. Adv.* **2020**, *6*, eabb1122.
[13] a) Z. Mao, S. Srinivasan, A. J. Appleby, *J. Appl. Electrochem.* **1992**, *22*, 693; b) J. Bressan, R. Wiart, *J. Appl. Electrochem.* **1979**, *9*, 43; c) R. Ichino, C. Cachet, R. Wiart, *Electrochim. Acta* **1996**, *41*, 1031; d) J. W. Diggle, A. Damjanovic, *J. Electrochem. Soc.* **1972**, *119*, 1649.
[14] a) A. Mitha, A. Z. Yazdi, M. Ahmed, P. Chen, *ChemElectroChem* **2018**, *5*, 2409; b) K. Zhao, F. Liu, G. Fan, J. Liu, M. Yu, Z. Yan, N. Zhang, F. Cheng, *ACS Appl. Mater. Interfaces* **2021**, *13*, 47650.
[15] a) K. Zhao, G. Fan, J. Liu, F. Liu, J. Li, X. Zhou, Y. Ni, M. Yu, Y.-M. Zhang, H. Su, Q. Liu, F. Cheng, *J. Am. Chem. Soc.* **2022**, *144*, 11129; b) X. Wang, M. Chen, S. Li, C. Zhao, W. Zhang, Z. Shen, Y. He, G. Feng, Y. Lu, *ACS Cent. Sci.* **2021**, *7*, 2029.
[16] a) Q. Zhang, J. Luan, Y. Tang, X. Ji, H. Wang, *Angew. Chem. Int. Ed.* **2020**, *59*, 13180; b) L. Miao, R. Wang, S. Di, Z. Qian, L. Zhang, W. Xin, M. Liu, Z. Zhu, S. Chu, Y. Du, N. Zhang, *ACS Nano* **2022**, *16*, 9667.
[17] Y. Yang, H. Hua, Z. Lv, M. Zhang, C. Liu, Z. Wen, H. Xie, W. He, J. Zhao, C. C. Li, *Adv. Funct. Mater.* **2023**, *33*, 2212446.
[18] N. Zhang, Y. Dong, M. Jia, X. Bian, Y. Wang, M. Qiu, J. Xu, Y. Liu, L. Jiao, F. Cheng, *ACS Energy Lett.* **2018**, *3*, 1366.

Manuscript received: February 28, 2023
Revised manuscript received: April 13, 2023
Accepted manuscript online: April 13, 2023
Version of record online: April 27, 2023